Title: **Neural Circuit Revision in Retinal Remodeling, A Pathoconnectomics Approach**

Authors: *Rebecca L Pfeiffer[1], Jeebika Dahal[1], Crystal L Sigulinsky[1], James R Anderson[1], Isabel A Barrera[1], Jia-Hui Yang[1], Olivia Haddadin[1], Alexis Houser[1], Jessica C Garcia[1], Bryan W Jones[1]*

1. Moran Eye Center/ Ophthalmology, University of Utah, Salt Lake City, Utah, United States

Corresponding Author: Rebecca L. Pfeiffer r.pfeiffer@utah.edu

Abstract: The Aii glycinergic amacrine cell (Aii) plays a central role in bridging rod pathways with cone pathways, enabling an increased dynamic range of vision from scotopic to photopic ranges. The Aii integrates scotopic signals via chemical synapses from rod bipolar cells (RodBCs) onto the arboreal processes of Aii ACs, injecting signals into ON-cone bipolar cells (CBbs) via gap junctions with Aiis on the arboreal processes and the waist of the Aii ACs. The CBbs then carry this information to ON and OFF ganglion cell classes. In addition, the Aii is involved in the surround inhibition of OFF cone bipolar cells (CBas) through glycinergic chemical synapses from Aii ACs onto CBas. We have previously shown changes in RodBC connectivity as a consequence of rod photoreceptor degeneration in a pathoconnectome of early retinal degeneration: RPC1. Here, we evaluated the impact of rod photoreceptor degeneration on the connectivity of the Aii to determine the impacts of photoreceptor degeneration on the downstream network of the neural retina and its suitability for integrating therapeutic interventions as rod photoreceptors are lost. Previously, we reported that in early retinal degeneration, prior to photoreceptor cell loss, Rod BCs make pathological gap junctions with Aiis. Here, we further characterize this altered connectivity and additional shifts in both the excitatory drive and gap junctional coupling of Aiis in retinal degeneration, along with discussion of the broader impact of altered connectivity networks. New findings reported here demonstrate that Aiis make additional gap junctions with CBas increasing the number of BC classes that make pathological gap junctional connectivity with Aiis in degenerating retina. In this study, we also report that the Aii, a tertiary retinal neuron alters their synaptic contacts early in photoreceptor degeneration, indicating that rewiring occurs in more distant members of the retinal network earlier in degeneration than was previously predicted. This rewiring impacts retinal processing, presumably acuity, and ultimately its ability to support therapeutics designed to restore image-forming vision. Finally, these Aii alterations may be the cellular network level finding that explains one of the first clinical complaints from human patients with retinal degenerative disease, an inability to adapt back and forth from photopic to scotopic conditions.

Introduction:

The glycinergic Aii amacrine cell (Aii) is a central node for visual processing in retinal networks (Marc et al., 2014). In healthy mammalian retina, the Aii mediates scotopic (low-light) vision by relaying signals from rod photoreceptor-connected rod bipolar cells (RodBCs) to ganglion cell-connected ON-cone bipolar cells (CBbs) by bridging chemical synapses with gap junctions, or electrical synapses (Famiglietti and Kolb, 1975; Marc et al., 2014; Masland, 2012). Additionally, the Aii engages in reciprocal synapses with OFF-cone bipolar cells (CBas), contributing to scotopic-driven OFF signaling, ON-OFF opponency, and rod-cone crossover opponency through the lateral inhibition of CBas (Strettoi et al., 1992). Additionally, studies have demonstrated extensive gap junctional coupling between Aiis (Feigenspan et al., 2001; Strettoi et al., 1992; Veruki and Hartveit, 2002), and that gap junctional coupling strength varies with luminance (Bloomfield et al., 1997; Hampson et al., 1992).

Aii function in rod-mediated scotopic vision pathways is easily observed. Given the paucity of direct synapses between RodBCs and ganglion cells in the healthy mammalian retina, the connection to the CBbs via gap junctions with the Aii is the primary mechanism by which light is perceived under scotopic conditions. When this pathway is disrupted, significant loss of scotopic vision occurs (Deans et al., 2002; Jin et al., 2022). The function of the Aii in ON-OFF and rod-cone crossover motifs are more subtle, yet is observable through psychophysical analysis of cone flicker threshold during rod adaptation. As rods reach a dark adaptation state, the intensity of light required for a subject to perceive a flicker via cone input is increased (Goldberg et al., 1983), presumably through inhibition of the cone pathway in the inner retina by the rod pathway. Additionally, Aiis participate in surround inhibition over most of the visual dynamic range except the most scotopic of conditions (Nath et al., 2023). Disruption of this pathway component has been observed in patients with Retinitis Pigmentosa and other rod dystrophies (Arden and Hogg, 1985).

Retinitis Pigmentosa (RP) is a retinal degenerative disease caused by numerous genetic mutations resulting in the progressive loss of rod photoreceptors (Hartong et al., 2006). Along with the loss of rods, the retina enters into a state of plasticity or negative remodeling (Jones et al., 2003). There are many components of retinal remodeling, including gliosis, cell death, cell migration, rewiring, and more, that taken together result in the global phenomenon of retinal remodeling that encompasses all retinal classes of neurons (Jones et al., 2012). Eventually, retinal remodeling progresses to late-stage neurodegenerative events where proteinopathies begin to assert themselves in much the same way as in CNS neurodegenerative diseases like Parkinson's or Alzheimer's disease (Pfeiffer et al., 2020c). Of particular relevance to this study, is the process of rewiring, in which neurons begin to make aberrant connections in the diseased retina (Fariss et al., 2000; Jones et al., 2011; Jones et al., 2003; Marc and Jones, 2003; Peng et al., 2000; Strettoi et al., 2003; Strettoi et al., 2002). During rewiring, it has been observed in advanced stages of retinal degeneration that neurons will extend neurite processes into different retina layers and make synapses with unknown partners (Jones et al., 2003). These findings are confirmed in animal models of retinal degeneration with genetic causes (Fariss et al., 2000; Peng et al., 2000; Strettoi et al., 2002), as well as induced non-genetic causes (Marc et al., 2008), and have been confirmed in human RP (Jones et al., 2016a) and AMD (Jones et al., 2016b) patients.

In 2020, our first ultrastructural pathoconnectome, Retinal Pathoconnectome 1: *RPC1* (Pfeiffer et al., 2020a) allowed us to interrogate, at synaptic resolution, the state of rewiring in the inner retina early in retinal degeneration. In this case, early retinal degeneration is defined as

following the onset of rod photoreceptor degeneration, but prior to broadly observed neurite outgrowth, complete rod loss, or observed cone photoreceptor stress. Our original hypothesis was that during the early stages of rewiring, there would be a loss of synaptic specificity in the RodBCs and that this loss would manifest with high levels of variability. Instead, we found alterations in synaptic specificity and network topologies were both predictable and stereotyped. These alterations include the emergence of novel networks, including gap junctions between RodBCs and Aiis (Pfeiffer et al., 2020a). This is significant because while altered coupling patterns could be inferred through RodBC glycine content (Jones et al., 2011; Jones et al., 2016a; Marc et al., 2008), Cx36 phosphorylation state (Ivanova et al., 2015), and the specific involvement of Cx36 gap junctions in spontaneous activity (Ivanova et al., 2016) in retinal degeneration; the precise gap junction partnerships altered in RD were not fully described nor directly observed. Indeed, gap junctions are never found in RodBCs in the healthy mammalian retina, but in early retinal degenerative disease, the rules and patterns of gap junctional connectivity are clearly altered. In this study, we continue our analysis of the corrupted network of RPC1 to understand the early consequences of rod degeneration on the inner retina, focusing on the Aii amacrine cell networks.

Materials and Methods:

Connectome and Pathoconnectome Volumes:

The healthy connectome: Retinal Connectome 1 (RC1) first published in 2009 (Anderson et al., 2009) and comprehensively described in 2011 (Anderson et al., 2011a) from a 13-month Dutch Belted female rabbit, contains 341 TEM sections, 18 CMP capstone (serial sections bookending the TEM volume) sections, and 11 intercalated CMP sections containing IgGs to GABA (γ), Glycine (G), Taurine (τ), Glutamate (E), and 1-amino-4-guanidobutane (AGB), which was loaded during the sample preparation. The pathoconnectome: Retinal Pathoconnectome 1 (RPC1) (Pfeiffer et al., 2020a) was generated from a 10-month transgenic P347L rabbit model of autosomal dominant retinitis pigmentosa (Jones et al., 2011; Kondo et al., 2009). RPC1 contains 946 TEM sections with 14 intercalated CMP sections. IgGs labeled in RPC1 include GABA (γ), Glycine (G), Taurine (τ), Glutamate (E), Glutamine (Q), and Glial Fibrillary Acidic Protein (GFAP) (Table 1). After enucleation, both volumes were prepared by fixing the tissues in mixed aldehydes (1% formaldehyde and 2.5% glutaraldehyde). Tissues were then osmicated, dehydrated in graded alcohols, and embedded in epon resins. Tissues were then serially sectioned on an ultramicrotome set to 70nm and placed on formvar grids for TEM capture or on slides for CMP analysis.

Computational Molecular Phenotyping (CMP)

Established identities of neurons in the volume are critical to understanding networks. Spatial metabolic fingerprints allow us to definitively identify cells in the volume as belonging to specific cell classes. Therefore, we include CMP analysis of small molecule and protein epitopes into each of our connectome or pathoconnectome volumes. CMP allows cell fingerprinting through the quantitative analysis of small molecule combinations, which are stoichiometrically trapped during fixation and detected with glutaraldehyde-tolerant IgGs (Marc and Jones, 2002; Marc et al., 1990; Marc et al., 1995). The inclusion of small molecules furthers the identification of neuronal types by adding the predominant neurotransmitter as a data point to the morphology and connectivity of a given neuron. Further background on the theory of CMP can be found in prior publications (Marc and Jones, 2002; Marc et al., 1995; Pfeiffer et al., 2020b).

Image Capture, Assembly, and Annotation:

Transmission electron microscopy (TEM) samples were imaged using a JEOL 1400 transmission electron microscope with a 16-Mpixel Gatan Ultrascan camera. TEM was selected because it provides high-resolution imaging (~2.18nm/px) with minimal dwell time. It also affords higher resolution recaptures with tilt for validation of individual structures such as gap junctions (Sigulinsky et al., 2020). Samples prepared for CMP were imaged using Leica DMR light microscopes with an 8-bit CCD camera, and Surveyor software.

RC1 was assembled using the NCR toolkit (Anderson et al., 2009), and RPC1 was built with a modern version of NCR Toolkit called Nornir (https://nornir.github.io/). This software assembles complete sections (mosaics) from tiled TEM or light-microscopy images and then performs semi-automated registration to align the serial sections with minimal manual correction (Anderson et al., 2009; Marc et al., 2012).

Following volume assembly, navigating the dataset and manual annotation are performed using the Viking software environment (Anderson et al., 2011b). Expert annotators manually annotate every synapse (chemical or electrical) according to the parameters outlined below in the Synapse Identification and Nomenclature section. Each of these annotations is recorded in a central database which encodes each structure's location, size, and linked partners (Anderson et al., 2009). We endeavor to minimize false positives or missed network connections through the complete annotation of all synapses. The annotation of all synapses is an audacious undertaking, and as more experts evaluate cells within a volume, missed structures may be found, leading to an evolving dataset. Both RC1 and RPC1 volumes are publicly available at https://websvc1.connectomes.utah.edu/RC1/OData/ and http://websvc1.connectomes.utah.edu/RPC1/OData.

Synapse Identification and Nomenclature:

To detail synaptic connectivity in this study, we will refer to chemical synapses as either conventional or ribbon synapses based on their ultrastructural morphology as previously described (Pfeiffer et al., 2020a). Conventional synapses are generally inhibitory synapses of classical synaptic structure: a pre-synaptic vesicle cloud opposing a post-synaptic density. The presence of a pre-synaptic ribbon characterizes ribbon synapses, and the ribbon may oppose one or more post-synaptic densities on neighboring neurons. Ribbon synapses of the inner retina are always excitatory. Gap junctional electrical synapses are also evaluated in this study and are identified through the distinct pentalaminar structure indicative of gap junctions (Pfeiffer et al., 2020a; Sigulinsky et al., 2020). While many gap junctions were identifiable at our native 2.18nm/pixel resolution, some were at an oblique orientation and required higher magnification recaptures with goniometric tilt. Recaptures were performed at 25,000x (0.43nm/pixel resolution).

Morphology Annotation and Rendering:

In order to more accurately present the morphology of the neurons presented in this paper, we deviated from our classical annotations using circles (Anderson et al., 2011b) and added in polygon annotation functionality. Here, we used a mix of circles (in cell bodies and descending processes) and polygons to more accurately represent the morphology of the neurons presented in this study.

To render the more complex morphologies created through the addition of polygons, it was necessary to create a new morphology rendering module of Viking: VikingMesh. VikingMesh is based on the methods generated by Bajaj and colleagues for volumetric feature extraction and

visualization (Bajaj et al., 2003). It improves the Bajaj methods by restricting mesh generation across sections to annotations (contours in the Bajaj terminology) known to be physically connected as recorded in the Viking database. Contour relationships were unknown in the original Bajaj inputs. Dae files were generated using the VikingMesh renderer, and were subsequentially passed through a screened Poisson surface remeshing algorithm (https://github.com/RLPfeiffer/VikingMesh_addons) harnessing the pymeshlab python library (https://pymeshlab.readthedocs.io/en/latest/). Dae files were then imported into Blender (https://www.blender.org/) and projection images to illustrate the 3D morphology and relationships were acquired, size metrics from the annotations is also preserved throughout the rendering process.

Data Analysis:

All data encoded in Viking annotations is automatically synced back to a central SQL database for each volume (Anderson et al., 2009; Anderson et al., 2011b). These databases encode not only location, sizing, and spatial relationships, but also synaptic partnerships (Anderson et al., 2011b). To evaluate the inputs, outputs, and partnerships between cells and synapses we utilized custom SQL stored procedures and pandas to pull and statistically evaluate the ribbon inputs and gap junction partners of the designated Aii cells in each volume (https://github.com/RLPfeiffer/VikingExplore). Graphs of the data were generated in Tableau (https://www.tableau.com).

Figure Generation:

Figures were assembled using screenshots from the RC1 (https://websvc1.connectomes.utah.edu/RC1/OData/) and RPC1 (https://websvc1.connectomes.utah.edu/RPC1/OData/) volumes in Viking (https://connectomes.utah.edu/) and projection images acquired in Blender as described above in Morphology Annotation and rendering. Final figure assembly was done in Photoshop 6.0

Results:

Gross Anatomy of Aii Cells:

RPC1 contains 11 Aiis. For this study, the 5 Aiis that are predominately contained within the volume (cells minimally have processes extending beyond the bounds of the volume) have been reconstructed (Cell #s 192, 262, 265, 1685, 2710). RC1 is a robust connectomics dataset generated from a healthy rabbit retina and has been extensively annotated, providing comprehensive descriptions of Aii connectivity motifs (Marc et al., 2014; Sigulinsky et al., 2020). All the Aiis contain moderate glycine levels, similar to that found within Aiis of retinal connectome 1: *RC1* (Marc et al., 2014) (Figure 1), consistent with prior studies (Marc and Liu, 1985; Pourcho and Goebel, 1985).

In addition to the similar glycine signature of Aiis in RPC1, the gross morphology of the Aii is comparable between the two datasets and consistent with the wider literature of Aii morphology. Namely, the Aiis in RPC1 retain clearly defined lobular and arboreal dendrites characteristic of the Aii cell type (Famiglietti and Kolb, 1975; Kolb and Famiglietti, 1974; Mills and Massey, 1991; Vaney, 1985) (Figure 1). The Aii's soma is located in the inner nuclear layer, directly adjacent to and partially pushing into the inner plexiform layer (IPL), wherein its dendrites stratify in both the OFF and ON layers. The lobular dendrites of the Aii extend within the OFF layer, with a distinct

pattern of narrow branches with interspersed, large, vesicle-rich lobules. The arboreal dendrites of the Aii project from the waist of the Aii deep into the ON layer of the IPL, stratifying in the lowest plexiform layers neighboring the ganglion cell layer.

Aii Core Motifs:

The Aii connectivity has been extensively characterized in the healthy retina (Marc et al., 2014; Sigulinsky et al., 2020; Strettoi et al., 1992; Tsukamoto and Omi, 2013, 2017). Based on this, we chose to evaluate three robustly described primary motifs, conserved across mammals, that are characteristic of Aii connectivity (Figure 2). The first motif evaluated was the chemical synapses between the Aii lobular dendrites and CBas. As initially described by Famiglietti and Kolb in 1975 (Famiglietti and Kolb, 1975), Aii lobules make chemical synapses onto neighboring CBas (later found to be using glycine as the primary inhibitory neurotransmitter (Marc and Liu, 1985; Pourcho and Goebel, 1985)). Aiis also receive ribbon input from neighboring CBas onto their lobules as originally shown by McGuire et al., 1984 (McGuire et al., 1984). Both the inhibitory synapses from the Aii and the excitatory synapses from CBas are found within the lobules of Aiis in RPC1 (Figure 2B-B'). The second motif we evaluated was the RodBC ribbon synapses onto Aiis. As previously established (Kolb and Famiglietti, 1974), RodBCs are heavily presynaptic to the Aii in the healthy retina. We find that this pathway is conserved in the degenerate retina as evidence by large ribbons made within the ON layer from RodBCs onto Aiis within RPC1 (Figure 2C). This motif is foundational to the rod pathway because the Aii is the only clear pathway for scotopic information to be passed from the RodBCs to the ganglion cells (Figure 2A). The third and last motif we evaluated was the gap junctional coupling between Aiis and CBbs (Figure 2D). Also initially described by Famiglietti and Kolb (Famiglietti and Kolb, 1975; Kolb and Famiglietti, 1974), and subsequentially detailed by numerous groups (Demb and Singer, 2012; Lauritzen et al., 2019; Marc et al., 2014; Massey and Mills, 1999b; Mills and Massey, 1995; Sigulinsky et al., 2020; Strettoi et al., 1992), this electrical synapse is the second part of the pathway from RodBCs to ganglion cells allowing for immediate transfer of scotopic vision from the rod pathway to the ON-cone pathway once the signal is relayed to the Aii. Although all three motifs are intact within RPC1, our previous study of the RodBCs revealed clear, ultrastructurally-proven aberrant gap junctional coupling between the Aii and RodBCs (Pfeiffer et al., 2020a). This result, combined with previous results indicating altered Aii circuitry in retinal degeneration (Euler and Schubert, 2015; Zeck, 2016) led us to question to what extent the frequency and/or strength of the gap junctional and excitatory input motifs are altered in the degenerate retina.

Motif Frequency:

Our first metric for evaluating the impact of retinal degeneration on Aii motifs was to analyze the synaptic frequency of ribbon inputs to the Aii and the number of gap junctions made by the Aii with its neuronal partners. Each synaptic pairing described is classified by motif and summarized below. All percentage frequencies are calculated by their percentage of all synapses of that type aggregated by volume and accompanied by the mean and standard deviation of the individual cells involved in the motif. The purpose of presenting both values is to describe the impact of rewiring on the inner retina both globally, by evaluating the motif by volume, while the per cell mean and standard deviation demonstrates the level of variability.

Ribbon Inputs

The first component of input frequency we evaluated was the ribbon inputs by the various classes of bipolar cells (Table 2). Although total ribbon input to Aiis is decreased in in RPC1 (RC1

total ribbon inputs per Aii: 116±12.71, RPC1 total ribbon inputs per Aii: 73.2±11.12), proper lamination is preserved and all bipolar cell superclasses (CBa, CBb, and RodBC) are found within the dataset (Figure 3A-3D).

RodBC → Aii

Extended analysis of previously identified Aiis in the healthy rabbit connectome (RC1) (Marc et al 2014) demonstrates a broad number of input RodBCs per individual Aii (10-15). In contrast, the number of RodBCs making ribbons onto Aiis in RPC1 is dramatically decreased to 6-10 RodBCs per Aii When tabulating numerical ribbon input from RodBCs onto Aiis, we find the total number of ribbons from RodBCs varies between 81 to 109 ribbon synapses per Aii cell, making up 83.37% (mean ± std: 83.39% ± 4.65, coefficient of variation (CV) = 0.05) of total ribbon input to Aiis in RC1 (Figure 3E-F). Further amplifying the observed decrease in RodBC ribbon input in RPC1, the total number of ribbons from RodBCs onto Aiis is reduced to 33-59 ribbons per Aii. This decrease, however, is not uniform across Aiis with the percentage of RodBC ribbon input onto Aiis in dropping to 67.47%, but coinciding with an increase in coefficient of variation (67.38% ± 9.52, CV= 0.13) (Figure 3E-F).

CBa → Aii

The next most common bipolar cell ribbon input partner to Aiis in the healthy retina are the CBa bipolar cells, which are responsible for transmitting OFF network information to the Aii (McGuire et al., 1984). In RC1, 6-13 individual CBas are presynaptic to each Aii. These CBas make a total of 10-19 ribbons onto each Aii, constituting 14.41% (14.37% ± 3.38, CV= 0.26) of the Aiis' total ribbon input (Figure 3E-F). In RPC1, the input from CBas is more variable with a total of 8-29 ribbons coming from 3-11 individual CBas presynaptic to each Aii. Overall, the relative input from the CBa superclass onto the Aiis of RPC1 increases to 23.66% (22.99% ± 8, CV=0.33) of the total ribbon contribution (Figure 3E-F).

CBb → Aii

The last contributor of ribbon synapses onto the Aii comes from the CBb superclass. The majority of synapses between Aiis and CBbs are via gap junctions (Sigulinsky et al., 2020). However, there are a small number of ribbons from CBbs to Aiis found in the healthy retina (Marc et al., 2014; Sigulinsky et al., 2020). In RC1, CBb ribbon inputs exist at a low rate of 0-4 ribbons per Aii, comprising 1.77% (2.29% ± 1.49, CV=0.65) of total ribbon synapses from up to 3 CBbs (Figure 3E-F). In RPC1, Aiis receive ribbons from as many as 7 CBb partner cells with a wide range of 1-11 ribbons constituting 7.80% (8.47% ± 7.45, CV=0.87) of all ribbon inputs to each Aii (Figure 3E-F).

Aii Gap Junctions

Aberrant gap junctions between RodBCs and Aiis were first ultrastructurally described in the RPC1 volume (Pfeiffer et al., 2020a). No gap junctions have ever been directly observed or described in the literature between RodBCs and Aiis in the adult mammalian retina, leading us to conclude their emergence in the RPC1 volume is secondary to retinal plasticity events and retinal remodeling induced by rod degeneration. However, in the previous study, we did not evaluate whether the emergence of RodBC gap junctions occurred along with changes in other gap junctional motifs made by the Aii. Here, we expand upon previous efforts to evaluate the gap junction motifs in the healthy and degenerate retina and explore the relative contributions by each gap junction partnership (Figure 4).

Aii::Aii

The most prevalent gap junction pairing of Aiis in the healthy retina is with other Aiis (Marc et al., 2014; Sigulinsky et al., 2020; Strettoi et al., 1992) (Figure 4C). The raw number of Aii homocellular gap junctions (gap junctions with cells of the same class) observed in RC1 is between 76 and 102 Aii::Aii gap junctions (Figure 4I). The contribution of the Aii::Aii motif to the total number of gap junctions is 62.2% (62.62% ± 4.93, CV= 0.07) (Figure 4J). In RPC1, this motif is reduced to 54.91% (Figure 4J) of the total gap junctions (Figure 4E), although the cell-to-cell variability is increased (55.19% ± 7.28, CV= 0.13). This is further demonstrated by each individual Aii making 42-59 homocellular gap junctions (Figure 4I).

Aii::CBb

The gap junctional coupling between Aiis and CBbs is critical for the connection of rod inputs to the ganglion cells because RodBCs are not presynaptic to ganglion cells (Famiglietti and Kolb, 1975; Strettoi et al., 1990) (Figure 2A). In RC1, the Aii::CBb pairing is the other prominent gap junction motif of the Aii (Marc et al., 2014; Sigulinsky et al., 2020) (Figure 4D). Although a wide raw number of gap junctions of this motif exist per cell (39-73) (Figure 4I), the contribution of this motif is 36.77% of the Aii gap junctions in RC1 (Figure 4J) (36.35% ± 4.64, CV=0.13). In the degenerate RPC1 retina, Aii::CBb gap junctions (Figure 4F) constitute a smaller fraction of the total gap junction population at 29.46% (Figure 4J) with higher variability (29.21% ± 7.55, CV=0.26) and a raw number of 21-41 gap junctions (Figure 4I).

RodBC :: Aii

These findings are among the most remarkable in early degenerate retina, providing a pathway for visual processing corruption. Although the emergence of gap junctions between Aiis and RodBCs are novel to the early stage degenerating retina (Pfeiffer et al., 2020a) (Figure 4G), their frequency is remarkably consistent at 8-10 gap junctions per Aii (Figure 4I). With the addition of these gap junctions to the degenerate network, RodBCs make up 9.82% of all gap junctions made by Aiis in RPC1 (Figure 4J), again with lower variability than many other observed motifs (9.89% ± 1.45, CV=0.15). All RodBCs making gap junctions with Aiis also continue making ribbon synapses onto the same Aiis (Figure 4G).

Other Aii pairings

We also find within RPC1 the rare occurrence of Aii::CBa gap junctional coupling, as evidence by 2 instances of this pairing (Figure 4H). In these instances, branches of a single CBa (Cell# 135) were found to make small gap junctions with the waist region of a neighboring Aii (Cell# 192). These are another motif that has not been observed within the healthy retina, however it was exceptionally rare constituting only 0.45% of all gap junctions (Figure 4J), in contrast with the aberrant gap junctions observed with RodBCs.

While the gap junction motif percentages are certainly altered by the addition of the RodBC::Aii motif in RPC1 (Figure 4J), part of the changes in relative contributions of the Aii::CBb and Aii::Aii motifs is the increase of unknown partners (Figure 4I). Unknown partners arise due

to branch fragments that cannot be followed, generally due to rapidly going off the edge of the volume. In RC1, unknown partners contributed 0.83% of all gap junctions with Aiis. In RPC1, this number increased to 4.69% (Figure 4J), likely due to the smaller diameter of the RPC1 volume. Additionally, there were 3 instances of bipolar cells that could not be identified. These incomplete classifications, however, only make up 5.36% of all of the gap junctions made by Aiis in RPC1.

Aii Synaptic Weighting:

Extending our understanding of network inputs based on synaptic tabulation from specific cell classes, we explored how potential differences in synapse size affect synaptic weighting, or the relative strength of contributions, of each motif in the healthy and degenerate retina. To better estimate the potential synaptic weight, we directly measured the area of gap junctions and post-synaptic densities (PSDs) opposing presynaptic ribbons. The concept that gap junction plaque size is a contributing measure of strength is previously established (Sigulinsky et al., 2020), although it is not possible to evaluate pore conformation, phosphorylation state, nor rectification from TEM analysis alone. Cortical brain spine size is strongly correlated with synaptic strength (de Vivo et al., 2017), while the size of the readily releasable pool is not (Branco et al., 2010), and spine size has been previously used by others as a measure of relative input (Sampathkumar et al., 2021). In the retina, spines are not formed at PSD sites necessitating another metric of strength. Given the spine volume being proportional to the area of the PSD (Harris and Stevens, 1989), we chose to measure the area of the PSD opposing ribbon-type synapses as a metric of synaptic weight (Equation 1).

$$t \cdot \sum_{i=1}^{n} l_i$$

Equation 1: Area of PSD from annotated densities. *n* = number of sections PSD density extends across, *l* = length of density on given section, *t* = thickness of section (set at 70nm based on section thickness of volume).

Ribbon Synapse Strength

As described above, we evaluated the area of all PSDs on Aiis opposing a ribbon density, allowing us to approximate the strength of bipolar cell glutamatergic input from each class (Figure 5). This was done as an extension of the ribbon count metrics used in the previous section to determine whether the observed alterations in ribbon input counts by bipolar cell class to the Aii is representative of true alterations in strength of glutamatergic drive.

RodBC -> Aii

Consistent with the raw counts of RodBC ribbon synapses onto Aiis of the healthy retina, quantification of PSD area indicates that RodBCs are the greatest contributor to Aiis of all BCs in both the healthy and degenerate retina. We find that RodBC-opposed PSDs account for 87.66% of all ribbon PSD area in RC1, with the average PSD being 0.03μm^2 ± 0.017. This input demonstrates the total RodBC input strength is roughly 4% higher than indicated from raw count alone. In RPC1, RodBC-opposed PSDs are substantially larger than in RC1 at 0.04μm^2 ± 0.025 accounting for 80.76% of all ribbon PSD area, a full 13% greater input strength than is indicated by ribbon synapse count alone. The PSD sizes in RPC1 potentially compensate for the lower

numbers of ribbon inputs, which may help to equalize the relative strength of RodBC input to the Aiis.

CBa -> Aii

Following the overwhelming input from RodBCs, the next greatest ribbon input comes from the CBa class. In RC1, CBa inputs make up 10.52% of the total ribbon PSD area with an average PSD size of 0.02μm^2 ± 0.013. In RPC1, CBa-opposed PSDs make up 12.91% of the total ribbon PSD area with an average area of 0.018μm ± 0.014. In both cases, the small size of the PSDs demonstrates a decrease in network weight from that indicated by ribbon-synapse count alone (14.41% in RC1 and 23.66% in RPC1).

CBb -> Aii

Lastly, CBb ribbon inputs onto Aiis are by far the smallest contributor of glutamatergic input. In RC1, the CBb-opposed PSDs make up 1.48% of all ribbon PSD area with an average size of 0.024μm^2 ± 0.018. This is comparable to the 1.77% input calculated from ribbon inputs alone. In RPC1, the CBb-opposed PSDs make up 5.84% of the total ribbon PSD area, down from 7.8% calculated from ribbon input count alone, with an average area of 0.018μm^2 ± 0.014. The contributions in RPC1, however, are highly variable between individual Aiis. CBb-opposed PSDs may make up as little as 0.36% of all ribbon input (seen on Aii Cell # 265), or as much as 16.46% (seen on Aii Cell # 262).

Aii Gap Junction Size

As described by Sigulinsky et al. 2020 and Marc et al. 2014, Aii gap junctions are exceedingly precise, both in coupling partners (as evidence by the lack of gap junction formation despite opportunity in specific bipolar cell classes) and in gap junction plaque size (Sigulinsky et al., 2020). Gap junction size has been shown to correlate with strength (Flores et al., 2012; Szoboszlay et al., 2016), and is tightly associated with retinal gap junction partner motifs (Sigulinsky et al., 2020). Here, we build upon the coupling rules established in RC1 (Marc et al., 2014; Sigulinsky et al., 2020), and report the relative contributions of gap junctions in the Aii network of RPC1 by cell superclass partner (Figure 6).

Aii::Aii

Consistent with gap junction motif frequency determined by raw count and previously published reports (Famiglietti and Kolb, 1975; Marc et al., 2014; Massey and Mills, 1999b; Sigulinsky et al., 2020; Strettoi et al., 1992), the strongest coupling motif remains the Aii in-class coupling with other Aiis. In RC1, the area of gap junctions between Aiis make up 74.65% of all gap junctional area with an average area of 0.12μm^2 ± 0.1. In RPC1, this motif is still the strongest contributor to the Aii coupling network, but has dropped substantially to 50.03% of all gap junctions by area. This is further highlighted by the average area being substantially smaller at 0.05μm^2 ± 0.04.

Aii::CBb

As described in the previous section, the Aii::CBb motif is the other primary gap junction motif found in the Aii gap junction network. In RC1, this motif accounts for 24.62% of total gap

junctions by area, with an average area of 0.065μm^2 ± 0.06. In RPC1, however, the contribution of the Aii::CBb motif is dramatically increased to 40.06% of total gap junctional area and an average area of 0.073μm^2 ± 0.054.

Aii::RodBC

The emergence of the RodBC::Aii gap junction motif in RPC1 was the major impetus for this analysis. As previously noted, there are no gap junctions of this motif in RC1, nor have any ever been found in a healthy adult mammalian retina, and represents and entirely new architecture, albeit pathological, but predictable and stereotyped. In RPC1, this motif accounts for 3.29-7.9% of the gap junctional area made by individual Aiis, with 5.32% contribution to total gap junction area. The average Aii::RodBC gap junction in RPC1 is 0.029μm^2 ± 0.02.

Other Aii pairings

Lastly, the emergent gap junctions between a CBa (Cell # 135) and a Aii (Cell # 192) are exceedingly small. Although this motif has not been observed in the healthy retina, in RPC1 these make up only 0.05% of the total gap junctional area.

The unknown and incompletely identified gap junctions of RC1 contribute a combined 0.72% of the total gap junction area in RC1. In RPC1, these incomplete partnerships account for 4.57% of the total gap junction area of the analyzed cells. The unidentified partners are likely higher in RPC1 due to the smaller diameter of the volume.

Discussion:

In this study, we investigated the impact of retinal degeneration on network topologies of Aiis in RPC1, a pathoconnectome of early-stage retinal degeneration in a rabbit model of retinitis pigmentosa. Rod photoreceptor cell loss is observable in this volume, but not complete, and there is no observable cone photoreceptor cell loss. These results were evaluated and compared with results from the healthy rabbit connectome RC1. RC1 has been continuously annotated for the last 15 years providing extensive information about the Aii networks in the healthy rabbit (Anderson et al., 2011a; Marc et al., 2014; Sigulinsky et al., 2020), in addition to decades of prior work in rabbit retina (Casini et al., 1995; Massey and Mills, 1999a; Massey et al., 1992; Strettoi et al., 1990; Strettoi et al., 1992; Vaney et al., 1991a; Vaney et al., 1991b). The primary components of the Aii network evaluated in this study are the ribbon inputs from the 3 superclasses of bipolar cells (RodBC, CBa, and CBb) and the gap junctional motifs generated from Aiis and their partners, primarily focusing upon the impact of retinal degeneration on Aii connectivity. Additionally, we expanded our evaluation of the network changes observed in the degenerate retina by including synapse size as a metric of synaptic weight. The graphical representation of the results of this study are presented in Figure 7.

Ribbon Input

Our findings demonstrate that the ribbon inputs from different bipolar cell superclasses to Aiis undergo significant changes in RPC1 compared to RC1. The reduction in RodBC inputs

based on count alone is partially compensated for through an increase in PSD sizes, indicating a marginal difference in input strength. Simultaneously, CBa inputs exhibit a notable increase in count, with consistent PSD sizes, while CBb inputs show a numerical increase with decreased PSD sizes. The observed variability in CBa and CBb inputs in RPC1 suggests potential rewiring processes associated with retinal degeneration.

Of these changes, there are a few key points we find especially noteworthy. The first of which is the increased cell to cell variability in these input measures in RPC1 when compared to RC1. We expect that this variability is highlighting ongoing changes in wiring associated with the progression of retinal degeneration, and will likely become more striking as we evaluate future pathoconnectomes. The second, is the apparent compensatory sizing of the Aii PSDs opposing RodBC ribbons. This suggests that some sort of Aii specific factors may be influencing the overall input strength of RodBCs in the rod network of RPC1, providing a normalization of the network input strengths, perhaps through a homeostatic plasticity mechanism. At its core, homeostatic plasticity is the drive of a neural system to return to a set point of function during and following a perturbation to the neural system. The potential for homeostatic plasticity in the retina has been extensively characterized by multiple investigators (Fitzpatrick and Kerschensteiner, 2023; Leinonen et al., 2020; Shen et al., 2020). Ultimately, the potential of the retina to compensate for both the loss of rod input along with the potential increase of cone photoreceptor inputs(Pfeiffer et al., 2020a; Whitaker et al., 2021) during the continuum of retinal degeneration will be an interesting test of the limits of homeostatic plasticity. Further research is required to elucidate the underlying mechanisms behind these observed changes in ribbon inputs; however, these results are immediately applicable to modeling efforts to understand the impact of network changes on retinal processing (Farzad, et al., 2023, Kosta, et al., 2021).

Gap Junctions

Previously, we reported the increase of gap junction partners of Aiis in degenerate retina to include RodBCs (Pfeiffer et al., 2020a). In this study, we more thoroughly characterize the Aii network changes in gap junction coupling patterns and describe the emergence of a novel motif, Aii gap junctions with the CBa class of bipolar cells. These results suggest an expanded rewiring of gap junction synapses in the degenerate retina, occurring prior to complete rod photoreceptor degeneration and preceding the more severe neurite outgrowth rewiring events.

We observed a dramatic decrease in the number of homocellular (Aii::Aii) gap junctions in RPC1. Homocellular gap junctions between Aiis are the most common gap junction motif made by Aiis, often found at the tips of arboreal dendrites. Although in RPC1, some of the evaluated Aiis went off the volume due to the limitations of the small diameter of the volume, this decrease in number did not fully account for the decrease in gap junctions. The total number of homocellular gap junctions was only marginally different between Aiis that went off volume (1685 & 262) and those that did not (2710 & 265). The only major exception to homocellular gap junction number was Aii 192. Aii 192 may represent a more advanced stage of rewiring as evidenced by its decrease in Aii::Aii gap junctions, its increase in Aii::CBb gap junctions, and the emergence of gap junctions with CBa 135. We report this with the acknowledgement that with only a single Aii demonstrating these characteristics, it may be an outlier. However, this connectivity pattern and the presence of gap junctions with a CBa have not been found in any other Aii indicating it may be part of the pathology. Future pathoconnectomics efforts in more advanced stages of degeneration will hopefully clarify this phenomenon.

Numerically, the emergence of gap junctions with RodBCs appears to have occurred with a roughly equivalent drop of both homocellular gap junctions with other Aiis and heterocellular gap junctions with CBbs. This data alone would suggest a simple addition of gap junction partnerships with RodBCs in RPC1. However, the numerical difference in gap junctions is only a part of the story, as illustrated by incorporating the information on gap junction size. From the size data, we now know that there is a decrease in the weight of input originating from Aii::Aii gap junctions coinciding with the emergence of the Aii::RodBC coupling and strengthening of the Aii::CBb coupling. This coupling shift indicates a potential narrowing of the spatial domains occupied by the Aii class and greater weight on the vertical component of visual processing (the passage of light detection information through the interneurons of the retina to the ganglion cell output neurons). Moreover, gap junctions in the Aii::CBb coupled network underlie oscillatory activity in ganglion cells of degenerating retinas that likely degrades vision (Zeck, 2016). Evidence for an increased open probability led to models of these oscillations that rely on changes in existing coupling motifs. The aberrant Aii::RodBC coupling motifs described herein provide an additional mechanism to be evaluated by future modeling efforts.

Finally, a glaring remaining question is the origin of the Aii::RodBC gap junctions. Gap junction connectivity in the retina is highly cell type- and partner type-specific, requiring expression, assembly, targeting and presentation of compatible connexons between coupled cells. Formation of intercellular gap junctions by mammalian RodBCs has not been reported in healthy retina. So where does the machinery come from to allow the formation of these aberrant intercellular gap junctions by rabbit RodBCs during degeneration? Certainly, there is evidence of reprogramming in degenerating bipolar cells and these RodBCs may be taking on another bipolar cell superclass phenotype (Jones et al., 2011; Marc et al., 2007), but which comes first – aberrant connections or gene expression? Of the 20+ mammalian connexin proteins, only five have been reported to be expressed by retinal neurons. Two of these (Cx50 and Cx57) are specific to horizontal cells (HC), while Cx36, Cx45, and Cx30.2 are expressed in multiple non-HC cell types (Reviewed in (Volgyi et al., 2013)). Connexon compatibility is necessary for intercellular channel formation and Aii ACs have thus far been shown to express Cx36 and Cx30.2, but not Cx45 (Deans et al., 2002; Guldenagel et al., 2001; Maxeiner et al., 2005; Meyer et al., 2016; Mills et al., 2001). Mouse reporter lines for specific connexins demonstrate PKCα-labeled RodBCs lack Cx36 reporter expression (Deans et al., 2002; Feigenspan et al., 2004), Cx45 reporter expression (Maxeiner et al., 2005) and Cx30.2 reporter expression (Meyer et al., 2016) in the mouse retina. Additionally, transcriptomic analyses support the lack of connexins Cx36 or Cx45 in mouse RodBCs (Shekhar et al., 2016). Despite this evidence against gap junction proteins in RodBCs across mammalian species, Mills and colleagues do report diffuse Cx36 cytoplasmic stain in the somas and axons of rabbit RodBCs (Mills et al., 2001). However, this staining lacked the puncta characteristic of intercellular gap junctions, consistent with our ultrastructural findings that RodBCs do not form gap junctions in healthy rabbit retina (this study, (Marc et al., 2014; Pfeiffer et al., 2020a; Sigulinsky et al., 2020)). While ultrastructural (Tsukamoto et al., 2001; Tsukamoto and Omi, 2013, 2017) and physiological (Fournel et al., 2021) studies support an absence of gap junction formation by RodBCs in other mammalian retinas, a candidate teleost RodBC homologue does form gap junctions. The rod-dominant PKCα-positive MB1-BCs of teleost retinas exhibit functional tracer and electrical coupling with neighboring MB1-BCs under both light- and dark-adapted conditions (Arai et al., 2010). Furthermore, gap junctions comprised of Cx35 (the teleost gene homolog of mammalian Cx36) are proposed to mediate this coupling, although there is discrepancy in whether these gap junctions are localized to the telodendria versus the distal dendrites of MB1-BCs in different species (Arai et al., 2010; O'Brien et al., 2004). Thus, it appears

possible that RodBCs may innately express the necessary machinery for gap junction formation. Whether there are conditions under which RodBCs normally utilize this or what triggers it during remodeling to form aberrant connections, remains unclear.

Summary:

In summary, our analysis demonstrated a shift in the ribbon input patterning and gap junctional coupling patterns in a degenerate retina. These shifts in patterning are initially evident in count-based analyses conducted using ultrastructural connectomics and pathoconnectomics methodologies. The impact of the changes in ribbon input and gap junction synaptologies are further clarified through the analysis of synaptic weight using size as the evaluation metric. This is significant because it helps to clarify where in remodeling the network begins to fail. As previously described, homeostatic plasticity is the mechanism by which an altered neural system may return to a homeostatic “set point”. This is perhaps illustrated in the shift in size of PSDs opposing RodBC ribbon in Aiis and the emergence of gap junctions as a mechanism to preserve scotopic vision despite progressive rod degeneration. However, given a long enough disease period, homeostatic plasticity fails and we may be seeing that failure start to occur in Aii 192 of the RPC1 pathoconnectome, early in the process of retinal degeneration. Identifying the points of system failure in remodeling will provide windows of opportunity for therapeutic intervention, and perhaps specific molecular targets for therapeutic intervention. This study provides insight into the mechanisms behind homeostatic plasticity and begins to characterize the points in which that process has failed.

Acknowledgements: The lab has been supported by the National Institutes of Health R01Grant EY028927 (BWJ), P30 Grant EY014800 (Core), the National Science Foundation NeuroNex2 Grant (2014862), an Unrestricted Research Grant from Research to Prevent Blindness, New York, NY to the Department of Ophthalmology & Visual Sciences, University of Utah, and an Unrestricted Research Grant from Gabe Newell (BWJ).

References

Anderson, J.R., Jones, B.W., Watt, C.B., Shaw, M.V., Yang, J.H., Demill, D., Lauritzen, J.S., Lin, Y., Rapp, K.D., Mastronarde, D., Koshevoy, P., Grimm, B., Tasdizen, T., Whitaker, R., Marc, R.E., 2011a. Exploring the retinal connectome. Mol Vis 17, 355-379.

Anderson, J.R., Jones, B.W., Yang, J.H., Shaw, M.V., Watt, C.B., Koshevoy, P., Spaltenstein, J., Jurrus, E., U, V.K., Whitaker, R.T., Mastronarde, D., Tasdizen, T., Marc, R.E., 2009. A computational framework for ultrastructural mapping of neural circuitry. PLoS Biol 7, e1000074.

Anderson, J.R., Mohammed, S., Grimm, B., Jones, B.W., Koshevoy, P., Tasdizen, T., Whitaker, R., Marc, R.E., 2011b. The Viking viewer for connectomics: scalable multi-user annotation and summarization of large volume data sets. J Microsc 241, 13-28.

Arai, I., Tanaka, M., Tachibana, M., 2010. Active roles of electrically coupled bipolar cell network in the adult retina. J Neurosci 30, 9260-9270.

Arden, G.B., Hogg, C.R., 1985. Rod-cone interactions and analysis of retinal disease. Br J Ophthalmol 69, 404-415.

Bajaj, C., Yu, Z., Auer, M., 2003. Volumetric feature extraction and visualization of tomographic molecular imaging. J Struct Biol 144, 132-143.

Bloomfield, S.A., Xin, D., Osborne, T., 1997. Light-induced modulation of coupling between AII amacrine cells in the rabbit retina. Vis Neurosci 14, 565-576.

Branco, T., Marra, V., Staras, K., 2010. Examining size-strength relationships at hippocampal synapses using an ultrastructural measurement of synaptic release probability. J Struct Biol 172, 203-210.

Casini, G., Rickman, D.W., Brecha, N.C., 1995. AII amacrine cell population in the rabbit retina: identification by parvalbumin immunoreactivity. J Comp Neurol 356, 132-142.

de Vivo, L., Bellesi, M., Marshall, W., Bushong, E.A., Ellisman, M.H., Tononi, G., Cirelli, C., 2017. Ultrastructural evidence for synaptic scaling across the wake/sleep cycle. Science 355, 507-510.

Deans, M.R., Volgyi, B., Goodenough, D.A., Bloomfield, S.A., Paul, D.L., 2002. Connexin36 is essential for transmission of rod-mediated visual signals in the mammalian retina. Neuron 36, 703-712.

Demb, J.B., Singer, J.H., 2012. Intrinsic properties and functional circuitry of the AII amacrine cell. Vis Neurosci 29, 51-60.

Euler, T., Schubert, T., 2015. Multiple Independent Oscillatory Networks in the Degenerating Retina. Front Cell Neurosci 9, 444.

Famiglietti, E.V., Jr., Kolb, H., 1975. A bistratified amacrine cell and synaptic cirucitry in the inner plexiform layer of the retina. Brain Res 84, 293-300.

Fariss, R.N., Li, Z.Y., Milam, A.H., 2000. Abnormalities in rod photoreceptors, amacrine cells, and horizontal cells in human retinas with retinitis pigmentosa. Am J Ophthalmol 129, 215-223.

Feigenspan, A., Janssen-Bienhold, U., Hormuzdi, S., Monyer, H., Degen, J., Sohl, G., Willecke, K., Ammermuller, J., Weiler, R., 2004. Expression of connexin36 in cone pedicles and OFF-cone bipolar cells of the mouse retina. J Neurosci 24, 3325-3334.

Feigenspan, A., Teubner, B., Willecke, K., Weiler, R., 2001. Expression of neuronal connexin36 in AII amacrine cells of the mammalian retina. J Neurosci 21, 230-239.

Fitzpatrick, M.J., Kerschensteiner, D., 2023. Homeostatic plasticity in the retina. Prog Retin Eye Res 94, 101131.

Flores, C.E., Nannapaneni, S., Davidson, K.G., Yasumura, T., Bennett, M.V., Rash, J.E., Pereda, A.E., 2012. Trafficking of gap junction channels at a vertebrate electrical synapse in vivo. Proc Natl Acad Sci U S A 109, E573-582.

Fournel, R., Hartveit, E., Veruki, M.L., 2021. Differential Contribution of Gap Junctions to the Membrane Properties of ON- and OFF-Bipolar Cells of the Rat Retina. Cell Mol Neurobiol 41, 229-245.
Goldberg, S.H., Frumkes, T.E., Nygaard, R.W., 1983. Inhibitory influence of unstimulated rods in the human retina: evidence provided by examining cone flicker. Science 221, 180-182.
Guldenagel, M., Ammermuller, J., Feigenspan, A., Teubner, B., Degen, J., Sohl, G., Willecke, K., Weiler, R., 2001. Visual transmission deficits in mice with targeted disruption of the gap junction gene connexin36. J Neurosci 21, 6036-6044.
Hampson, E.C., Vaney, D.I., Weiler, R., 1992. Dopaminergic modulation of gap junction permeability between amacrine cells in mammalian retina. J Neurosci 12, 4911-4922.
Harris, K.M., Stevens, J.K., 1989. Dendritic spines of CA 1 pyramidal cells in the rat hippocampus: serial electron microscopy with reference to their biophysical characteristics. J Neurosci 9, 2982-2997.
Hartong, D.T., Berson, E.L., Dryja, T.P., 2006. Retinitis pigmentosa. The Lancet 368, 1795-1809.
Ivanova, E., Yee, C.W., Baldoni, R., Jr., Sagdullaev, B.T., 2016. Aberrant activity in retinal degeneration impairs central visual processing and relies on Cx36-containing gap junctions. Exp Eye Res 150, 81-89.
Ivanova, E., Yee, C.W., Sagdullaev, B.T., 2015. Increased phosphorylation of Cx36 gap junctions in the AII amacrine cells of RD retina. Front Cell Neurosci 9, 390.
Jin, N., Tian, L.M., Fahrenfort, I., Zhang, Z., Postma, F., Paul, D.L., Massey, S.C., Ribelayga, C.P., 2022. Genetic elimination of rod/cone coupling reveals the contribution of the secondary rod pathway to the retinal output. Sci Adv 8, eabm4491.
Jones, B.W., Kondo, M., Terasaki, H., Lin, Y., McCall, M., Marc, R.E., 2012. Retinal remodeling. Jpn J Ophthalmol 56, 289-306.
Jones, B.W., Kondo, M., Terasaki, H., Watt, C.B., Rapp, K., Anderson, J., Lin, Y., Shaw, M.V., Yang, J.H., Marc, R.E., 2011. Retinal remodeling in the Tg P347L rabbit, a large-eye model of retinal degeneration. J Comp Neurol 519, 2713-2733.
Jones, B.W., Pfeiffer, R.L., Ferrell, W.D., Watt, C.B., Marmor, M., Marc, R.E., 2016a. Retinal remodeling in human retinitis pigmentosa. Exp Eye Res 150, 149-165.
Jones, B.W., Pfeiffer, R.L., Ferrell, W.D., Watt, C.B., Tucker, J., Marc, R.E., 2016b. Retinal Remodeling and Metabolic Alterations in Human AMD. Front Cell Neurosci 10, 103.
Jones, B.W., Watt, C.B., Frederick, J.M., Baehr, W., Chen, C.K., Levine, E.M., Milam, A.H., Lavail, M.M., Marc, R.E., 2003. Retinal remodeling triggered by photoreceptor degenerations. J Comp Neurol 464, 1-16.
Kolb, H., Famiglietti, E.V., 1974. Rod and cone pathways in the inner plexiform layer of cat retina. Science 186, 47-49.
Kondo, M., Sakai, T., Komeima, K., Kurimoto, Y., Ueno, S., Nishizawa, Y., Usukura, J., Fujikado, T., Tano, Y., Terasaki, H., 2009. Generation of a transgenic rabbit model of retinal degeneration. Invest Ophthalmol Vis Sci 50, 1371-1377.
Lauritzen, J.S., Sigulinsky, C.L., Anderson, J.R., Kalloniatis, M., Nelson, N.T., Emrich, D.P., Rapp, C., McCarthy, N., Kerzner, E., Meyer, M., Jones, B.W., Marc, R.E., 2019. Rod-cone crossover connectome of mammalian bipolar cells. J Comp Neurol 527, 87-116.
Leinonen, H., Pham, N.C., Boyd, T., Santoso, J., Palczewski, K., Vinberg, F., 2020. Homeostatic plasticity in the retina is associated with maintenance of night vision during retinal degenerative disease. Elife 9.
Marc, R.E., Anderson, J.R., Jones, B.W., Sigulinsky, C.L., Lauritzen, J.S., 2014. The AII amacrine cell connectome: a dense network hub. Front Neural Circuits 8, 104.
Marc, R.E., Jones, B.W., 2002. Molecular phenotyping of retinal ganglion cells. J Neurosci 22, 413-427.

Marc, R.E., Jones, B.W., 2003. Retinal remodeling in inherited photoreceptor degenerations. Mol Neurobiol 28, 139-147.
Marc, R.E., Jones, B.W., Anderson, J.R., Kinard, K., Marshak, D.W., Wilson, J.H., Wensel, T., Lucas, R.J., 2007. Neural reprogramming in retinal degeneration. Invest Ophthalmol Vis Sci 48, 3364-3371.
Marc, R.E., Jones, B.W., Lauritzen, J.S., Watt, C.B., Anderson, J.R., 2012. Building retinal connectomes. Curr Opin Neurobiol 22, 568-574.
Marc, R.E., Jones, B.W., Watt, C.B., Vazquez-Chona, F., Vaughan, D.K., Organisciak, D.T., 2008. Extreme retinal remodeling triggered by light damage: implications for age related macular degeneration. Mol Vis 14, 782-806.
Marc, R.E., Liu, W.L., 1985. (3H) glycine-accumulating neurons of the human retina. J Comp Neurol 232, 241-260.
Marc, R.E., Liu, W.L., Kalloniatis, M., Raiguel, S.F., van Haesendonck, E., 1990. Patterns of glutamate immunoreactivity in the goldfish retina. J Neurosci 10, 4006-4034.
Marc, R.E., Murry, R.F., Basinger, S.F., 1995. Pattern recognition of amino acid signatures in retinal neurons. J Neurosci 15, 5106-5129.
Masland, R.H., 2012. The neuronal organization of the retina. Neuron 76, 266-280.
Massey, S.C., Mills, S.L., 1999a. Antibody to calretinin stains AII amacrine cells in the rabbit retina: double-label and confocal analyses. J Comp Neurol 411, 3-18.
Massey, S.C., Mills, S.L., 1999b. Gap junctions between AII amacrine cells and calbindin-positive bipolar cells in the rabbit retina. Vis Neurosci 16, 1181-1189.
Massey, S.C., Mills, S.L., Marc, R.E., 1992. All indoleamine-accumulating cells in the rabbit retina contain GABA. J Comp Neurol 322, 275-291.
Maxeiner, S., Dedek, K., Janssen-Bienhold, U., Ammermuller, J., Brune, H., Kirsch, T., Pieper, M., Degen, J., Kruger, O., Willecke, K., Weiler, R., 2005. Deletion of connexin45 in mouse retinal neurons disrupts the rod/cone signaling pathway between AII amacrine and ON cone bipolar cells and leads to impaired visual transmission. J Neurosci 25, 566-576.
McGuire, B.A., Stevens, J.K., Sterling, P., 1984. Microcircuitry of bipolar cells in cat retina. J Neurosci 4, 2920-2938.
Meyer, A., Tetenborg, S., Greb, H., Segelken, J., Dorgau, B., Weiler, R., Hormuzdi, S.G., Janssen-Bienhold, U., Dedek, K., 2016. Connexin30.2: In Vitro Interaction with Connexin36 in HeLa Cells and Expression in AII Amacrine Cells and Intrinsically Photosensitive Ganglion Cells in the Mouse Retina. Front Mol Neurosci 9, 36.
Mills, S.L., Massey, S.C., 1991. Labeling and distribution of AII amacrine cells in the rabbit retina. J Comp Neurol 304, 491-501.
Mills, S.L., Massey, S.C., 1995. Differential properties of two gap junctional pathways made by AII amacrine cells. Nature 377, 734-737.
Mills, S.L., O'Brien, J.J., Li, W., O'Brien, J., Massey, S.C., 2001. Rod pathways in the mammalian retina use connexin 36. J Comp Neurol 436, 336-350.
Nath, A., Grimes, W.N., Diamond, J.S., 2023. Layers of inhibitory networks shape receptive field properties of AII amacrine cells. Cell Rep 42, 113390.
O'Brien, J., Nguyen, H.B., Mills, S.L., 2004. Cone photoreceptors in bass retina use two connexins to mediate electrical coupling. J Neurosci 24, 5632-5642.
Peng, Y.W., Hao, Y., Petters, R.M., Wong, F., 2000. Ectopic synaptogenesis in the mammalian retina caused by rod photoreceptor-specific mutations. Nat Neurosci 3, 1121-1127.
Pfeiffer, R.L., Anderson, J.R., Dahal, J., Garcia, J.C., Yang, J.H., Sigulinsky, C.L., Rapp, K., Emrich, D.P., Watt, C.B., Johnstun, H.A., Houser, A.R., Marc, R.E., Jones, B.W., 2020a. A pathoconnectome of early neurodegeneration: Network changes in retinal degeneration. Exp Eye Res 199, 108196.
Pfeiffer, R.L., Marc, R.E., Jones, B.W., 2020b. Muller Cell Metabolic Signatures: Evolutionary Conservation and Disruption in Disease. Trends Endocrinol Metab 31, 320-329.

Pfeiffer, R.L., Marc, R.E., Jones, B.W., 2020c. Persistent remodeling and neurodegeneration in late-stage retinal degeneration. Prog Retin Eye Res 74, 100771.
Pourcho, R.G., Goebel, D.J., 1985. A combined Golgi and autoradiographic study of (3H)glycine-accumulating amacrine cells in the cat retina. J Comp Neurol 233, 473-480.
Sampathkumar, V., Miller-Hansen, A., Murray Sherman, S., Kasthuri, N., 2021. An ultrastructural connectomic analysis of a higher-order thalamocortical circuit in the mouse. Eur J Neurosci 53, 750-762.
Shekhar, K., Lapan, S.W., Whitney, I.E., Tran, N.M., Macosko, E.Z., Kowalczyk, M., Adiconis, X., Levin, J.Z., Nemesh, J., Goldman, M., McCarroll, S.A., Cepko, C.L., Regev, A., Sanes, J.R., 2016. Comprehensive Classification of Retinal Bipolar Neurons by Single-Cell Transcriptomics. Cell 166, 1308-1323 e1330.
Shen, N., Wang, B., Soto, F., Kerschensteiner, D., 2020. Homeostatic Plasticity Shapes the Retinal Response to Photoreceptor Degeneration. Curr Biol 30, 1916-1926 e1913.
Sigulinsky, C.L., Anderson, J.R., Kerzner, E., Rapp, C.N., Pfeiffer, R.L., Rodman, T.M., Emrich, D.P., Rapp, K.D., Nelson, N.T., Lauritzen, J.S., Meyer, M., Marc, R.E., Jones, B.W., 2020. Network Architecture of Gap Junctional Coupling among Parallel Processing Channels in the Mammalian Retina. J Neurosci 40, 4483-4511.
Strettoi, E., Dacheux, R.F., Raviola, E., 1990. Synaptic connections of rod bipolar cells in the inner plexiform layer of the rabbit retina. J Comp Neurol 295, 449-466.
Strettoi, E., Pignatelli, V., Rossi, C., Porciatti, V., Falsini, B., 2003. Remodeling of second-order neurons in the retina of rd/rd mutant mice. Vision Res 43, 867-877.
Strettoi, E., Porciatti, V., Falsini, B., Pignatelli, V., Rossi, C., 2002. Morphological and functional abnormalities in the inner retina of the rd/rd mouse. J Neurosci 22, 5492-5504.
Strettoi, E., Raviola, E., Dacheux, R.F., 1992. Synaptic connections of the narrow-field, bistratified rod amacrine cell (AII) in the rabbit retina. J Comp Neurol 325, 152-168.
Szoboszlay, M., Lorincz, A., Lanore, F., Vervaeke, K., Silver, R.A., Nusser, Z., 2016. Functional Properties of Dendritic Gap Junctions in Cerebellar Golgi Cells. Neuron 90, 1043-1056.
Tsukamoto, Y., Morigiwa, K., Ueda, M., Sterling, P., 2001. Microcircuits for night vision in mouse retina. J Neurosci 21, 8616-8623.
Tsukamoto, Y., Omi, N., 2013. Functional allocation of synaptic contacts in microcircuits from rods via rod bipolar to AII amacrine cells in the mouse retina. J Comp Neurol 521, 3541-3555.
Tsukamoto, Y., Omi, N., 2017. Classification of Mouse Retinal Bipolar Cells: Type-Specific Connectivity with Special Reference to Rod-Driven AII Amacrine Pathways. Front Neuroanat 11, 92.
Vaney, D.I., 1985. The morphology and topographic distribution of AII amacrine cells in the cat retina. Proc R Soc Lond B Biol Sci 224, 475-488.
Vaney, D.I., Gynther, I.C., Young, H.M., 1991a. Rod-signal interneurons in the rabbit retina: 2. AII amacrine cells. J Comp Neurol 310, 154-169.
Vaney, D.I., Young, H.M., Gynther, I.C., 1991b. The rod circuit in the rabbit retina. Vis Neurosci 7, 141-154.
Veruki, M.L., Hartveit, E., 2002. AII (Rod) amacrine cells form a network of electrically coupled interneurons in the mammalian retina. Neuron 33, 935-946.
Volgyi, B., Kovacs-Oller, T., Atlasz, T., Wilhelm, M., Gabriel, R., 2013. Gap junctional coupling in the vertebrate retina: variations on one theme? Prog Retin Eye Res 34, 1-18.
Whitaker, C.M., Nobles, G., Ishibashi, M., Massey, S.C., 2021. Rod and Cone Connections With Bipolar Cells in the Rabbit Retina. Front Cell Neurosci 15, 662329.
Zeck, G., 2016. Aberrant Activity in Degenerated Retinas Revealed by Electrical Imaging. Front Cell Neurosci 10, 25.

Figures:

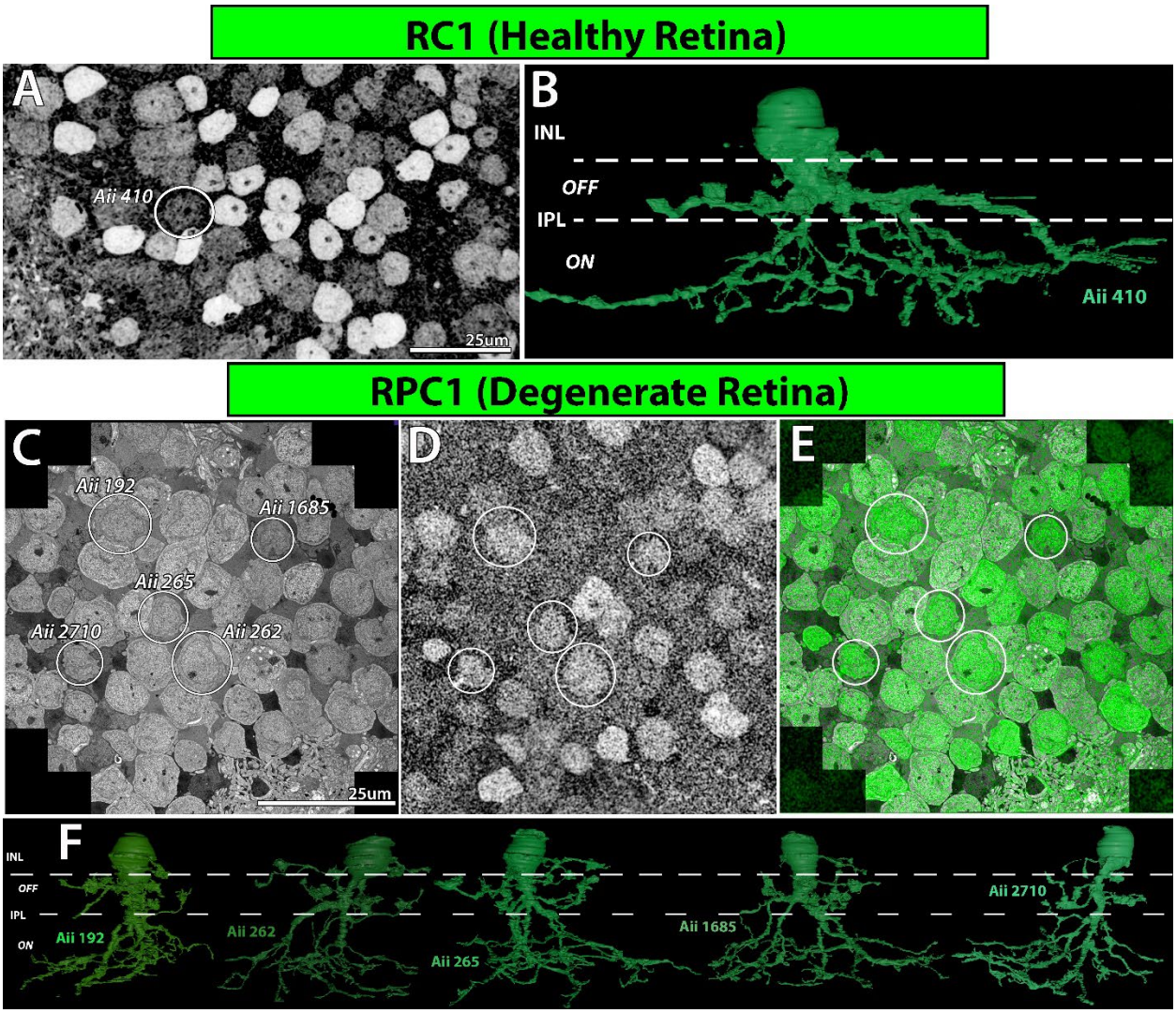

Figure 1: Aii Morphology and Glycine Content. (A) Glycine-labeled section (section 30) demonstrated the medium levels of glycine found in RC1 Aiis, including evaluated Aii 410 (circle). (B) 3D projection of rendered morphology of Aii 410 from RC1 data with markings illustrating retinal layers occupied by the cell. (C) TEM section (section 650) with Aiis evaluated in RPC1 circled and labeled. (D) Section adjacent (section 649) to the TEM section in C labeled for glycine, medium levels of glycine are consistent with Aii classification. (E) Overlay of images in C and D. (F) 3D projections of rendering of morphology of the 5 Aiis characterized in this study with layers of retina annotated.

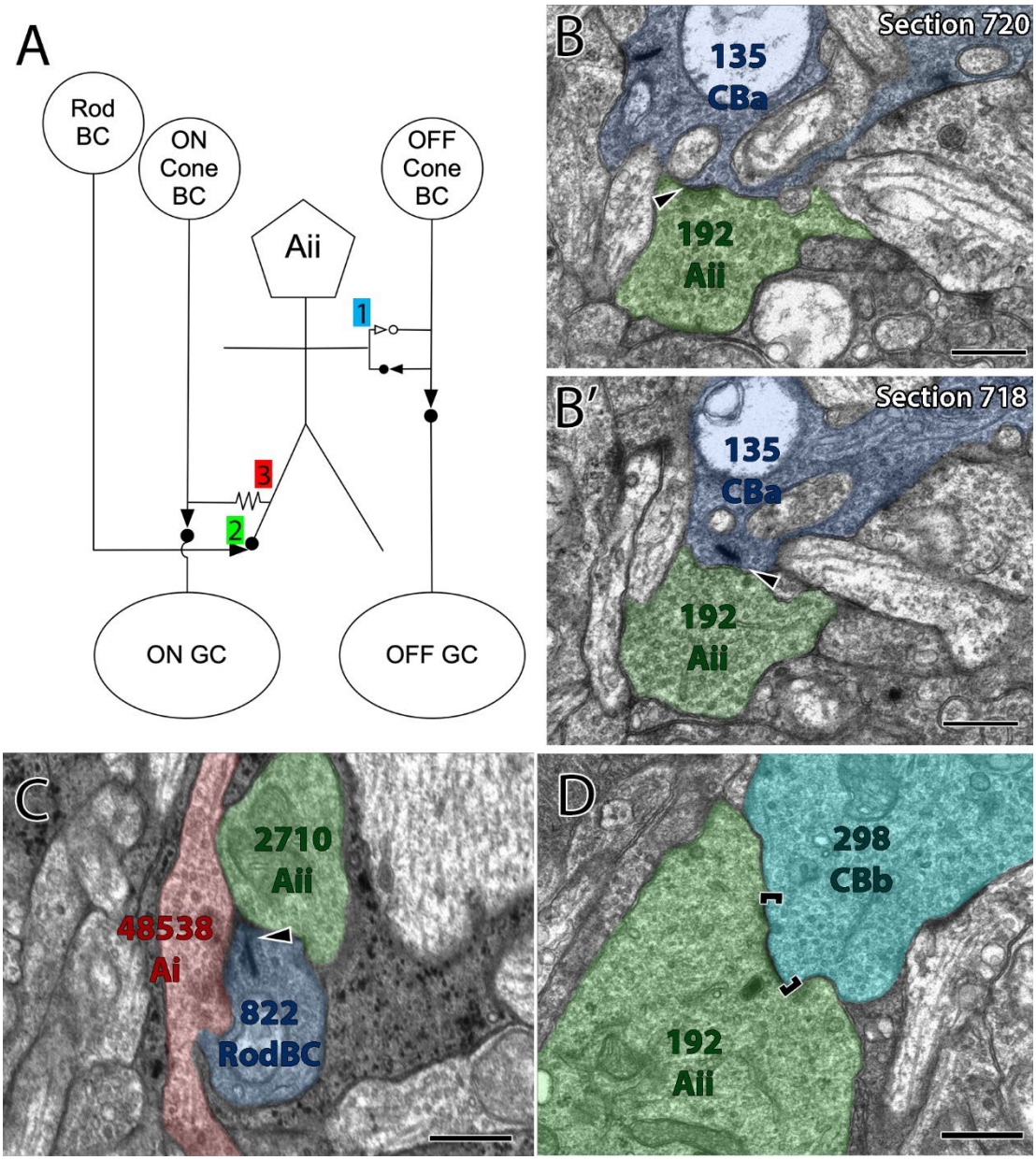

Figure 2: Canonical Aii Network Motifs are preserved in RPC1. (A) Network diagram of simplified Aii connectivity for passage of information of the primary rod pathway. 1: reciprocal synapses made with OFF-cone bipolar cells (CBa), 2: ribbon inputs from rod bipolar cells (RodBCs), 3: gap junctions with ON-cone bipolar cells (CBb). (B) Representative reciprocal synapse illustrating glycinergic conventional synapse from an Aii cell onto a Cba, and (B') a ribbon synapse from that same CBa onto the same Aii a few sections away. (C) Black arrow highlights ribbon synapse from a RodBC onto a Aii (D) Gap junction between an Aii and a CBb (represented by brackets). *Scale bars: 500nm*

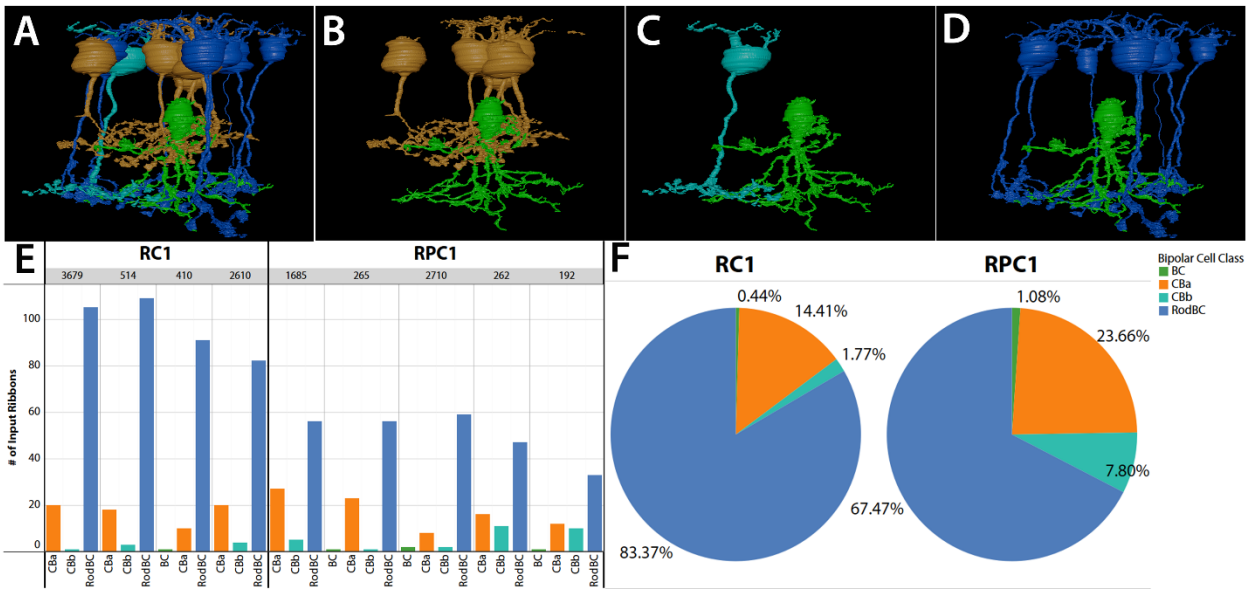

Figure 3: Numerical Counts of Ribbon Inputs onto Aiis. (A) 3D projection images of Aii 265 (green) and the bipolar cells that make ribbons onto it. (B) CBas (gold) presynaptic to Aii 265. (C) CBb (teal) presynaptic to Aii 265. (D) RodBCs (dark blue) presynaptic to Aii 265. (E) Number of input ribbons from each bipolar cell superclass onto each evaluated Aii. (F) Percentage of total ribbon input onto the evaluated Aiis organized by volume.

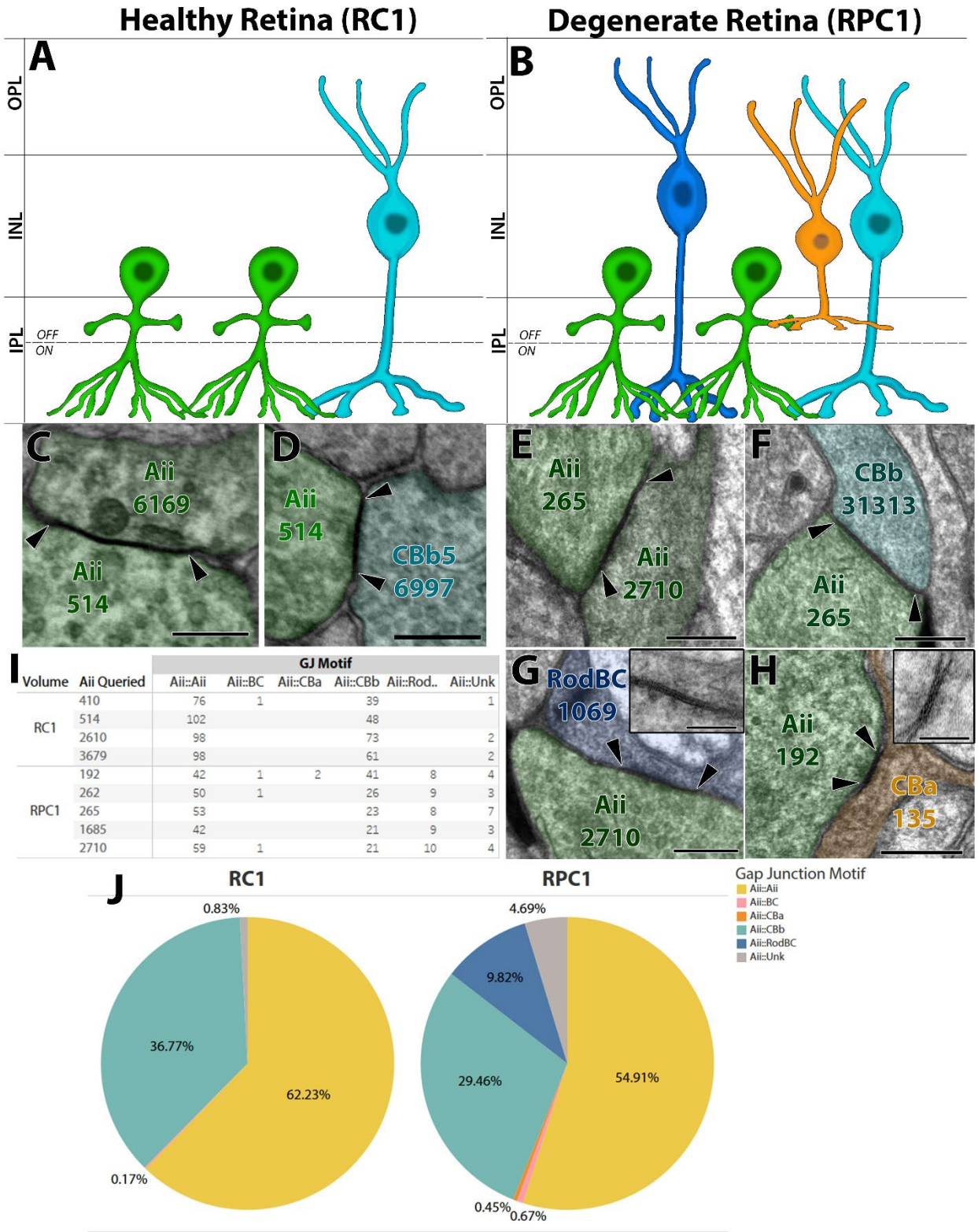

Volume	Aii Queried	GJ Motif					
		Aii::Aii	Aii::BC	Aii::CBa	Aii::CBb	Aii::Rod..	Aii::Unk
RC1	410	76	1		39		1
	514	102			48		
	2610	98			73		2
	3679	98			61		2
RPC1	192	42	1	2	41	8	4
	262	50	1		26	9	3
	265	53			23	8	7
	1685	42			21	9	3
	2710	59	1		21	10	4

Figure 4: Gap Junction Motifs and Frequency. (A) Diagram illustrating cell classes coupled with Aiis in the Healthy retina. (B) Diagram illustrating cells coupled with Aiis in the degenerate retina. (C-D) Gap junctions of both motifs present in the healthy retina, (C) Aii :: Aii and (D) Aii :: CBb. (E-H) Representative gap junctions present in RPC1 (E) Aii:: Aii, (F) Aii :: CBb, (G) Aii :: RodBC,

inset image: Higher magnification recapture @ 25k with 20 degree tilt, (H) Aii :: CBa *inset image*: High magnification recapture @ 25k with 4 degree tilt. (I) Raw counts of the gap junction motifs per analyzed cell in each volume. (H) Percentage of total number of gap junctions contributed by each motif. (scale bars *Primary panels: 250nm, inset images 100nm)*

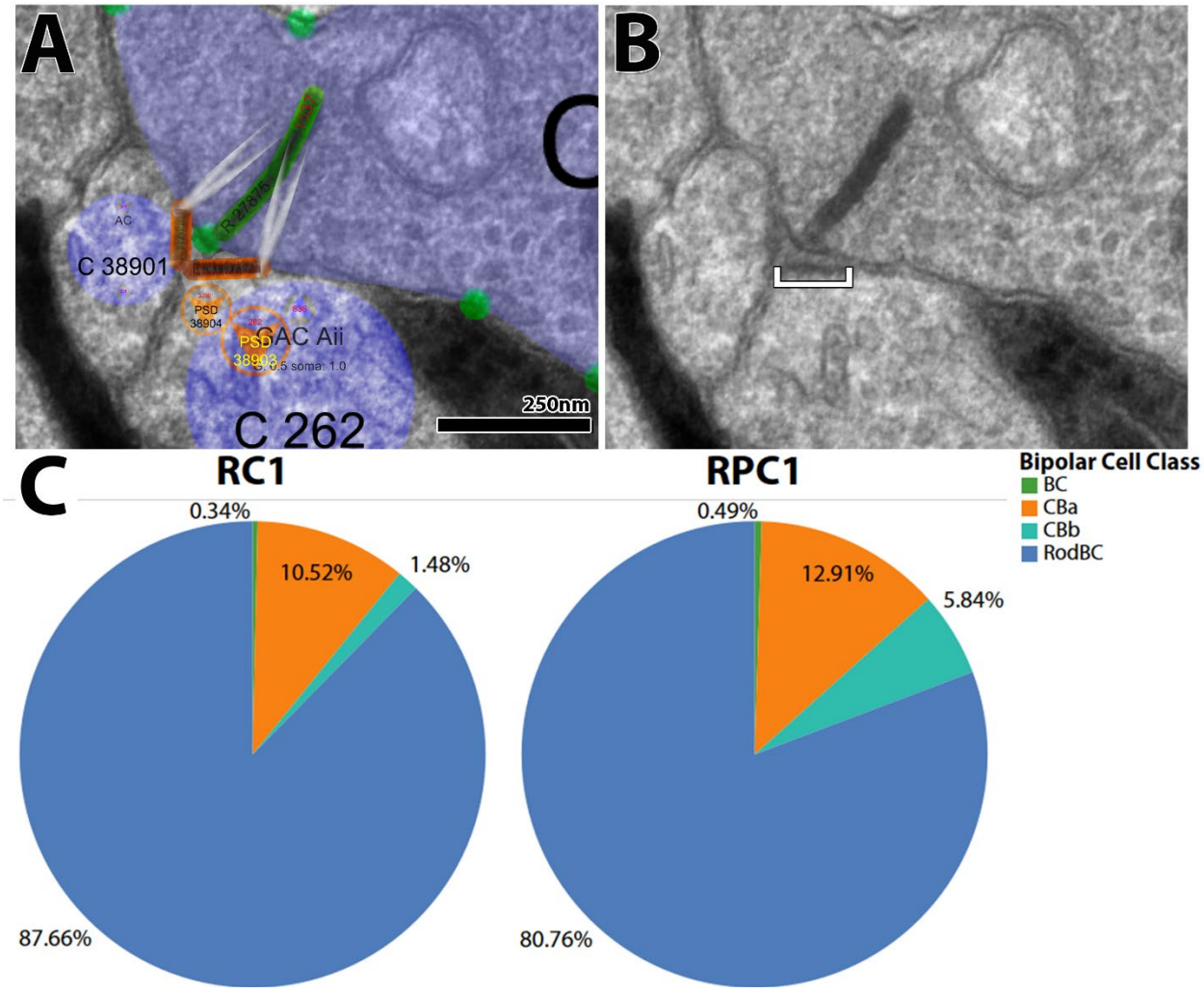

Figure 5: Ribbon Strength. (A) Annotated section demonstrating use of annotations to determine size. Green bar: ribbon, orange bar: annotated PSD, orange circles: references to annotations on adjacent sections. (B) Same section as shown in panel A without annotations. PSD is indicated by white bracket. (C) Percentage of contribution by each motif per volume as calculated by total gap junctional area.

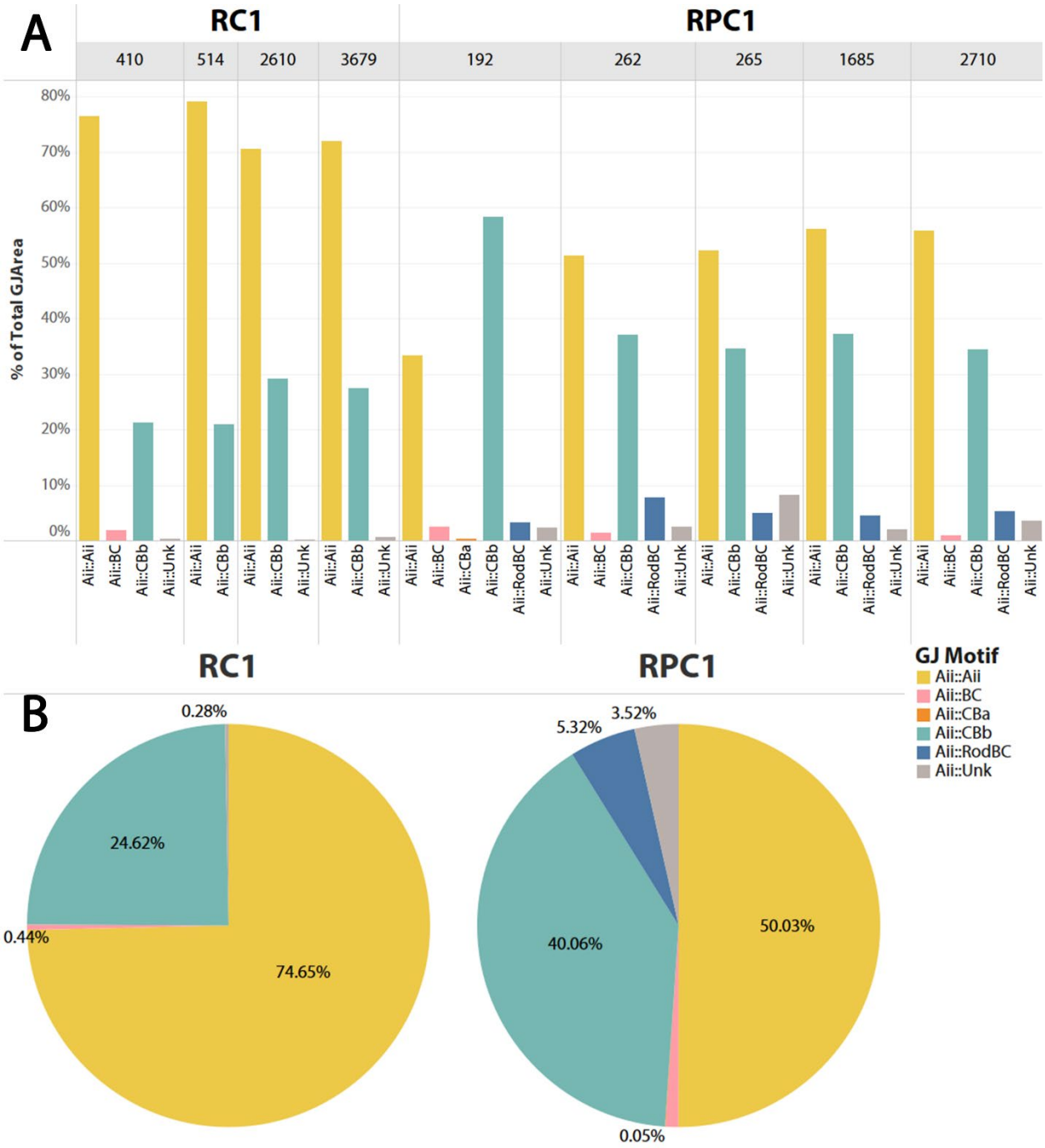

Figure 6: Gap Junction Strength. (A) Percentage of gap junction area contributed by each motif separated by cell and volume. (B) Percentage of total gap junction area contributed by each motif per volume.

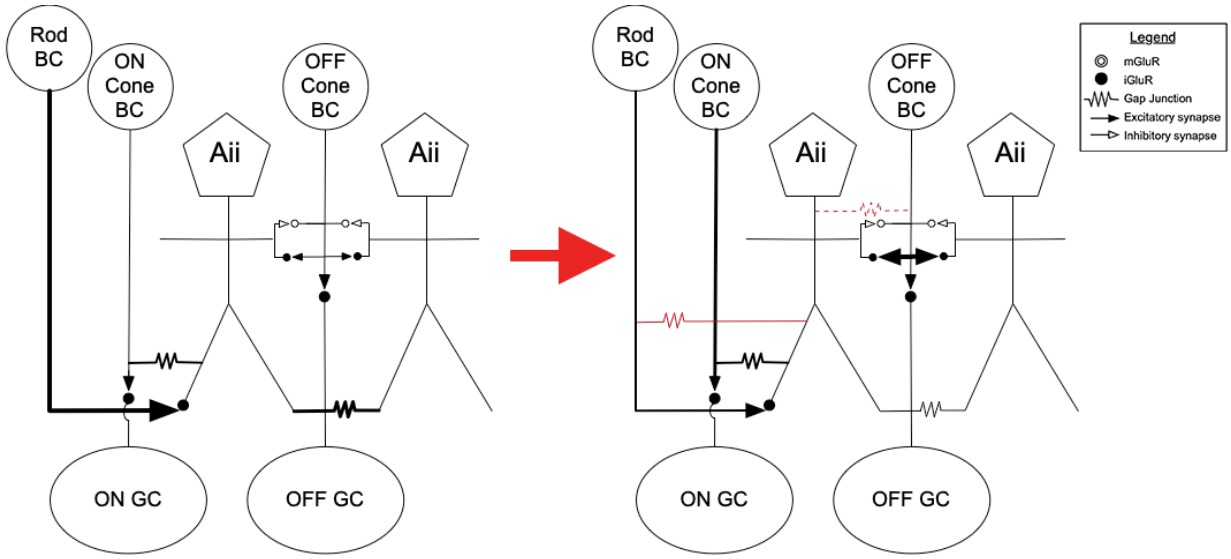

Figure 7: Circuit Diagram Illustrating Changes to Aii Contributions to Rod Network. Left panel is the healthy network. Right panel indicates the state of the altered network in RPC1. Weighting of lines indicates strength of input and red indicates connections only present in the degenerate retina.

Tables:

Table 1: List of Labels in RPC1

Reagent	RRID	Source	Dilution
anti-L-glutamate IgG	AB_2532055	Signature Immunologics	1:50
anti-glycine IgG	AB_2532057	Signature Immunologics	1:50
anti-L-glutamine IgG	AB_2532059	Signature Immunologics	1:50
anti-taurine IgG	AB_2532060	Signature Immunologics	1:50
anti-GABA IgG	AB_2532061	Signature Immunologics	1:50
anti-GFAP	AB_10013382	Dako	1:200

Table 2: Ribbon Input by Cell Type

		Bipolar Cell Class							
		BC		CBa		CBb		RodBC	
Volume	Aii Target	% of Total Ribbon Contributions	Ribbon Count	% of Total Ribbon Contributions	Ribbon Count	% of Total Ribbon Contributions	Ribbon Count	% of Total Ribbon Contributions	Ribbon Count
RC1	410	0.98%	1.0	9.80%	10.0			89.22%	91.0
	514			13.85%	18.0	2.31%	3.0	83.85%	109.0
	2610			18.87%	20.0	3.77%	4.0	77.36%	82.0
	3679			15.87%	20.0	0.79%	1.0	83.33%	105.0
RPC1	192	1.79%	1.0	21.43%	12.0	17.86%	10.0	58.93%	33.0
	262			21.62%	16.0	14.86%	11.0	63.51%	47.0
	265	1.23%	1.0	28.40%	23.0	1.23%	1.0	69.14%	56.0
	1685			30.68%	27.0	5.68%	5.0	63.64%	56.0
	2710	2.82%	2.0	11.27%	8.0	2.82%	2.0	83.10%	59.0